Model-Augmented Energy-Flow Reference for High-Delay Telemanipulation

Michael Panzirsch[1], Nicolai Bechtel[1], Thomas Hulin[1,2]

Abstract—**With increasing dexterity and robustness of robotic manipulation systems, their field of applications expands. Due to the still limited capabilities of autonomous agents and the requirement of fallback solutions in case of failure, teleoperation remains an essential functionality for systems that are far remote or in, for humans, inaccessible areas. Recently, a new control approach (TDPA-HD) was developed for teleoperation at extreme delays which ensures safe interactions, but, leads to conservative and late force application of the robot in its environment. In this work, we amalgamate the TDPA-HD with a model-augmentation approach to overcome this limitation and accelerate the force application without sacrificing the safety in the remote robotic interactions. To this end, we make use of a local virtual model of the remote environment which is pre-known or is sensed and created during runtime. Considering the energetic behavior of the haptic interaction of an operator with this local model as a reference for the remote interaction, the robot is allowed to apply interaction forces earlier when compared to pure TDPA-HD. At the same time, safe interactions in case of unexpected contacts with unmodeled objects in the remote environment are ensured. The method is introduced in 6-DoF and validated in 3-DoF experiments in rigid and elastic environments involving complex interaction tasks at up to 1.6s roundtrip-delay.**

Index Terms—**Passivity, Model-Mediated Teleoperation, Time Delay, MATM**

I. Introduction

Recent plans of larger space agencies involve planetary exploration with the help of mobile robots [1]. Still, the capabilities of autonomous robots are so far limited and especially sensor-based functionalities not fully robust. As a fallback solution [2] and in order to extend the capabilities of the robots, astronauts in an orbiting spacecraft will be equipped with a teleoperation interface to control robotic rovers and manipulators [3], [4] (compare Fig. 1). In such scenarios, the delay in the communication between robot and haptic interface exceeds the roundtrip-delay (RTD) of approximately 800ms in a geostationary link from Earth to International Space Station (ISS).

Manuscript received: July 19, 2023; Revised: October 31, 2023; Accepted: January 18, 2024. This paper was recommended for publication by Editor Angelika Peer upon evaluation of the Associate Editor and Reviewers' comments. The research work was partially funded by the German Research Foundation (DFG, Deutsche Forschungsgemeinschaft) as part of Germany's Excellence Strategy – EXC 2050/1 – Project ID 390696704 – Cluster of Excellence "Centre for Tactile Internet with Human-in-the-Loop" (CeTI) of Technische Universität Dresden. The work was partially funded by the Bavarian Ministry of Economic Affairs, Regional Development and Energy, within the project SMiLE2gether(LABAY102).

[1]M. Panzirsch, N. Bechtel and T. Hulin are with the Institute of Robotics and Mechatronics in the German Aerospace Center (DLR), Wessling, Germany. michael.panzirsch@dlr.de

[2]T. Hulin is with the Centre for Tactile Internet with Human-in-the-Loop (CeTI), Cluster of Excellence at TU Dresden, Dresden, Germany

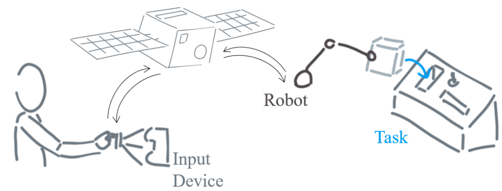

Fig. 1: Human operator with input device and robot.

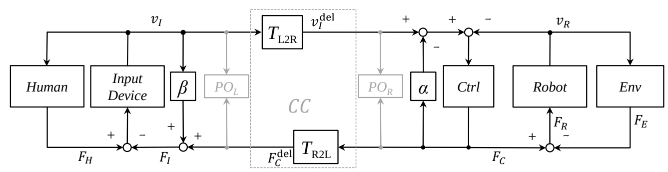

Fig. 2: Signal flow diagram of the conventional TDPA.

In order to execute manipulation tasks with contacts safely, displaying force feedback on the input device is of utmost importance. In addition to the force information for the astronaut itself, transmitting interaction forces enables preventing unexpected or hard impacts on the environment [5], [6] as will be explained later in more detail. The major challenge in force-feedback teleoperation is the delayed communication which presents an active element potentially leading to instability due to energy generation.

Different control approaches have been developed to enable stable telemanipulation despite of delay – among them the wave variables method [7], the Time Domain Passivity Approach (TDPA, [8]) or frequency-domain approaches as the Llewellyn absolute stability criterion [9]. Still, the transparency of the teleoperation setup (i.e. the feeling of immersion of the operator into the robot's environment) is heavily reduced with increasing delay. For some approaches the position tracking quality is reduced [7] while for most approaches also the force feedback (FF) quality is heavily attenuated or suffers from too high damping (position-position architectures [9], [10]). Frequency-Domain-based approaches as the Raisbeck, Llewellyn or Routh-Hurwitz criterion don't apply adaptive but constant damping which results in a mostly highly conservative parametrization and thus in weak performance. But, even the performance of the conventional TDPA [8] as one of the most commonly used in space robotics degrades heavily with increasing delay.

Recently, we proposed a new TDPA for high delays (TDPA-HD, [5], [6]) which achieves high position tracking accuracy and safe interactions independent of the communication delay [6]. That work presents a detailed comparison of TDPA and

 DOI: 10.1109/LRA.2024.3362155

TDPA-HD. Although [5] presented the successful completion of a variety of applications from sample picking and insertion to maintenance-related tasks at 3s roundtrip-delay (approximately Earth-to-Moon communication), the FF quality was limited by the control method. Furthermore, the time until a desired force is applied against the environment by the robot after first contact (from here referred to as 'time-to-interact' t_{TI}) is increased by the safety mechanism of the control approach.

This work proposes a combination of the TDPA-HD and the Model-Augmented Haptic Telemanipulation (MATM [11]) to overcome these two downsides i.e. to increase the FF quality and reduce the time-to-interact. MATM, in general, envisages integrating a local (operator side) and/or a remote (robot side) virtual model of the robot environment to ease interactions with this remote environment. The local model supports visual or haptic augmentation while the remote model can serve shared control functionalities. A large variety of augmented reality-enhanced human-robot interaction methodologies have been proposed in literature [12]. Most of these works related to telemanipulation focus on model-based force rendering [13], [14] and model-updates [15], [16] for environments of varying complexity [17].

Here, we observe the interaction with a local model (which can be a pre-known model or a point-cloud scanned in the remote environment) to determine a reference energy that can be applied in the remote interaction between the teleoperated robot and its environment. An exemplary application can be found in satellite maintenance which is investigated, for instance, in the DLR AI-In-Orbit-Factory 4.0 project [18]. In such scenarios, the robot is interacting with a pre-known or structured environment which can be well modeled. More precisely, this work aims the reduction of the time-to-interact in TDPA-HD. Therefore, the local MATM model is applied to observe an energy reference for the remote interaction. The operator interacts with a local virtual reality (VR) perceiving the rendered force on the input device. From the interaction, the energy that is intentionally applied against the modeled environment by the operator can be observed. This energy is then regarded as a reference for the remote interaction allowing earlier force application against the remote environment. Thus, the time-to-interact is reduced, while the TDPA-HD still ensures safe interactions in unexpected collisions against non-modeled objects. This paper focuses on investigating the stability of the haptic channel, i.e. the VR is only used for force rendering but not for visual rendering. Thus, the operator sees the camera video stream from the remote side.

The paper is structured as follows: Section II introduces the principles of the conventional TDPA, the TDPA-HD and the respective drawbacks. The concept and the integration of the TDPA-HD into the MATM framework is presented in Section III. 3-DoF experiments at 1.6s RTD communication delays in environments of varying complexity are presented in Section IV. Finally, Section V concludes the work.

II. Fundamentals and Problem Statement

The control circuit of a standard teleoperation setup is presented in Fig. 2. There, a human operator uses an input device to control a robot in a remote environment (Env.). A coupling PD controller (Ctrl) with spring-damper characteristics ensures the position tracking of the two devices. Therefore, a force is computed (F_C) from the Cartesian 6-DoF position and velocity difference of the devices. This force is applied locally at the robot and displayed on the input device (force feedback). The position and velocity reference of the input device v_I and the FF are delayed by time delays T_{L2R} and T_{R2L} respectively of the communication channel (CC). The Time Domain Passivity Approach (TDPA) serves the stabilization of the closed control loop despite communication delay. To this end, it observes the energy which is introduced by the CC (potentially causing instability) with passivity observers (PO) and dissipates excessive energy via passivity controllers (PC) with variable damping α and β. For this sake, the impedance-type $PC1$ with damping β attenuates the FF, while the admittance-type $PC2$ with damping α adapts the velocity command.

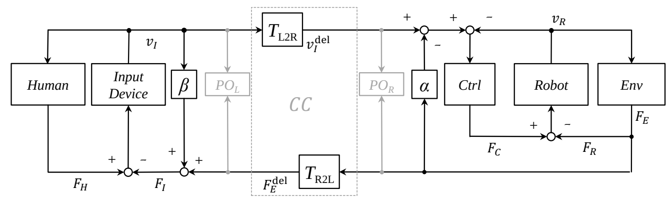

Fig. 3: Signal flow diagram of TDPA-HD [5].

As discussed before, even the performance (FF quality and position tracking) of the conventional TDPA reduces critically with increasing delay. In such passivity-based approaches, the problem arises from the large time shift between

- the time t_1 in which a force F_C is commanded to the robot by the remote coupling controller Ctrl,
- the time $t_2 = t_1 + T_{\mathrm{R2L}}$ in which this force (of the respective time step) is displayed at the input device (from which the energy input from the operator is determined) and
- the time $t_3 = t_2 + T_{\mathrm{L2R}}$ in which the energy input related to $F_C(t_1)$ arrives at the remote side.

Simplified, in the conventional TDPA [8], the velocity commanded by the operator is heavily attenuated by the passivity controller $PC2$ at $t = [t_1, t_3]$ since the remote side was not informed with how much power the robot may interact with the environment. Thereby, as long as the energy output on the robot side is higher than the respective energy input on the operator side, the passivity controller $PC2$ of the TDPA prevents a deflection of the $Ctrl$ spring and thus pressing against a contact or the motion of the robot. With increasing delay, the performance of the conventional TDPA decreases considerably, especially since computed controller forces F_C (which are also present during free motion) are considered for passivity control. These forces are non-zero during free motion phases thus causing power flow and also PC dissipation during free motion.

This problem was immensely reduced by the TDPA-HD for high delay telemanipulation [5]. The signal flow diagram of Fig. 3 explains the functionality of the TDPA-HD. Here, in contrast to the conventional TDPA, the force F_E measured by

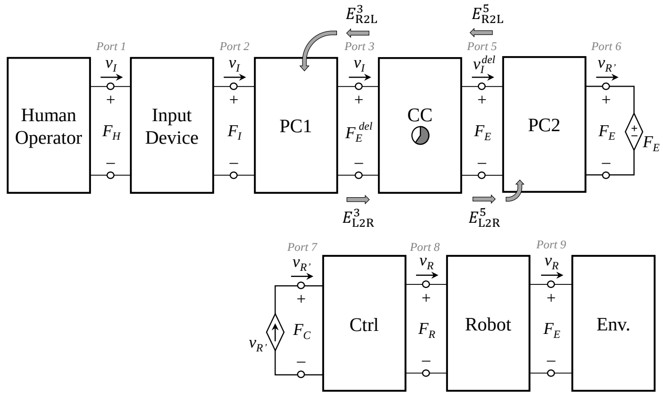

Fig. 4: Network representation of TDPA-HD [6].

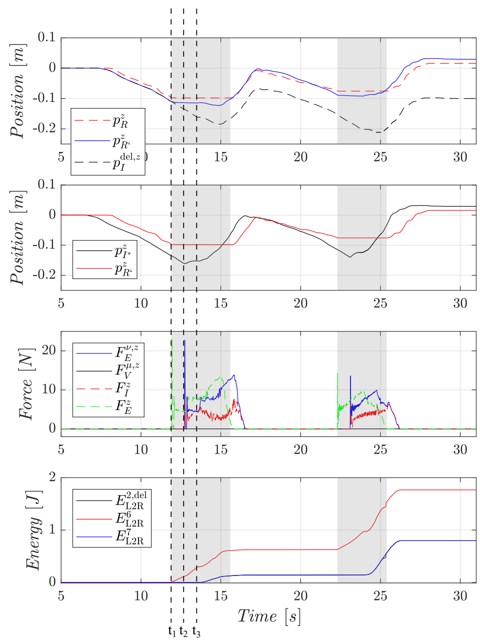

Fig. 5: Two wall contacts at 1.6s RTD with TDPA-HD.

a 6-DoF force-torque sensor at the robot endeffector is applied for passivity observation and control.

Fig. 4 presents the network representation of the teleoperation system described in Fig. 3. This diagram consists of 1- and 2-port subsystems connected via port interfaces at which an effort (force v) and a flow (velocity v) can be measured. Thus, at each port i a power flow P^i can be calculated as $P^i(k) = F^i(k)v^i(k)$ in each time step k. The sign of the power P^i determines whether the respective power flows in left-to-right (L2R, P^i_{L2R}) or right-to-left (R2L, P^i_{R2L}) direction. Note that the direction-specific sign of the power depends on the sign convention of the coupling controller. Via discrete time integration, the energies E^i_{L2R} and E^i_{R2L} can be calculated. Thus, the energy generation of the CC in each energy flow direction can be determined and considered for passivity control. Note that the port numbers are chosen according to the one in the later figures.

In TDPA-HD, $PC2$ limits the output energy at port 6 according to the energy input $E^3_{\text{L2R}}(t - T_{\text{L2R}})$ in L2R energy-flow direction. Thereby, E^3_{L2R} is observed from the input device velocity v_I and the delayed measured force F_E^{del} on the operator side. Thus, the robot follows perfectly in free motion (when $F_E = 0$), but stops at a contact with the environment (t_1) until the operator has perceived the contact (t_2) and the desired input/interaction power E^3_{L2R} has arrived on the remote side at t_3. On the one hand, this leads to highly safe interactions and avoidance of hard impacts. Furthermore, the robot position following shows very high performance in free motion since, in such zero-force phases, the admittance type $PC2$ needs to dissipate no energy. On the other hand, the TDPA-HD cannot avoid that the robot starts a desired interaction with the environment only after $t_{\text{TI}} = t_3 - t_1 = T_{\text{L2R}} + T_{\text{R2L}}$.

Figure 5 presents an experiment with TDPA-HD. Note that the poses presented in the plot are measured on the remote robot side to ease interpretation. The difference d_{PC2} between input device motion p_I^{del} and the commanded robot motion $p_{R'}$ indicates the drift induced by the admittance-type PC of TDPA-HD. This drift reduces the severity of unexpected collisions, because it prevents collision forces from being commanded to the remote robot in such situations (as described in [6] in detail), but it leads to delayed force application (time-to-interact t_{TI}) in case of desired interactions with the environment in the same way. The shaded area marks the time of the wall contacts. Note that due to delay, the force F_I displayed at the input device pushes the operator away from the wall, although the wall contact is already over at $t > 15.6s$ and $t > 25.4s$ respectively.

III. Proposed Approach

The main focus of the proposed approach lies on the reduction of time-to-interact t_{TI} while maintaining the safety aspects of the TDPA-HD in case of unexpected collisions. Therefore, we propose to apply a VR model of the remote environment with which the operator interacts locally. Through haptic rendering [19], the operator can perceive the virtual interaction and decide how much power should be applied against modeled objects. As depicted in Fig. 6, from this interaction an energy E^{VR} or power P^{VR} can be determined which represents the energy that the operator intentionally applies $against$ the environment. Transmitting this energy with the motion command to $PC2$ on the robot side, the robot may directly apply the respective force against the environment thus reducing the time-to-interact extensively. Still, as visualized in Fig. 7, contacts with non-modeled objects ($P^{\text{VR}} = 0$) are avoided for the time span of $t_{\text{TI}} = t_3 - t_1$ ensuring safety in interaction since $PC2$ ensures that the power P^{ENV} applied against the remote environment remains zero during t_{TI}.

A. Concept Description

The signal flow diagram of Fig. 8 presents the integration of the virtual model (VR) of the robot environment into the control loop on the operator-side of the TDPA-HD. The delayed position and velocity respectively of the input device p_I^{del} is the motion reference for the robot side coupling controller (Ctrl). The FF to the human operator is calculated

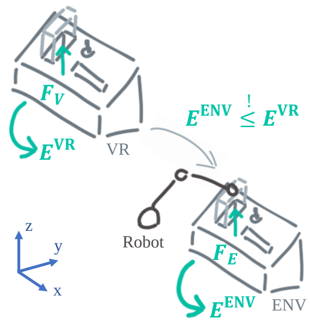

Fig. 6: Reference energy from VR interaction.

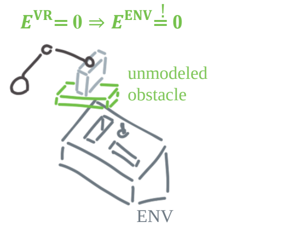

Fig. 7: Zero reference energy from VR in case of non-modeled obstacle.

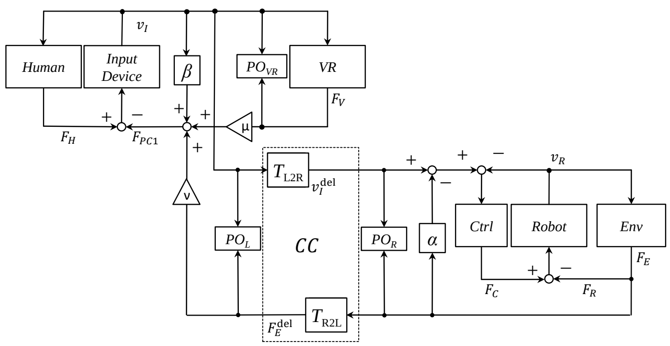

Fig. 8: Signal flow diagram of the proposed concept.

from the interaction force F_V rendered in VR and the delayed force feedback F_E^{del}:

$$F_I = F_{Ia} + F_{Ib} = \mu F_V + (1-\mu)F_E^{\text{del}}. \tag{1}$$

Here, we apply the haptic rendering algorithm of [20] with a god-object heuristic, with which collisions behave like linear springs in the direction of the collision. It is important to note that unlike to pure VR-scenarios, the god-object method is only used to compute the spring-like forces, but not for visualization. In case of extreme delay and comparably fast motions, the mismatch of forces F_{Ia} and F_{Ib} increases. To ensure sufficient transparency in such situations, the feedback force F_{Ib} can be reduced when the respective contact was expected. Thus, only during unexpected contacts, when F_{Ia} is zero, the operator would receive F_{Ib}.

As visualized in the respective network representation in Fig. 9, the energy $E^2_{\text{L2R}} = E^{4a}_{\text{L2R}} + E^{4b}_{\text{L2R}}$ is sent in L2R direction to the robot-side $PC2$ as the energy input reference representing the energy with which the user aims to interact with the VR. Here, $E_{\text{VR}} = E^{4a}_{\text{L2R}}$ and $E_{\text{ENV}} = E^7_{\text{L2R}}$.

B. Passivity Discussion

The energy observation and control can be split up into L2R and R2L direction. In L2R direction, PC2 considers the observed energy $W^{\text{PC2}}_{\text{obs}}$ for passivity control:

$$\begin{aligned} W^{\text{PC2}}_{\text{obs}}(k) = (&\mu E^{5a}_{\text{L2R}}(k - T_{\text{L2R}}) + \nu E^{5b}_{\text{L2R}}(k - T_{\text{L2R}})) \\ &- E_{\text{out}}(k) - E^{\text{PC2}}(k-1), \end{aligned} \tag{2}$$

with the output energy $E_{\text{out}} = E^6_{\text{L2R}}$ at port 6 and the energy E^{PC2} that was already dissipated by $PC2$. In R2L direction, PC1 limits E^2_{R2L} to the scaled energy input sum from VR and the remote side:

$$\begin{aligned} W^{\text{PC1}}_{\text{obs}}(k) = (&\mu E^{5a}_{\text{R2L}}(k) + \nu E^7_{\text{R2L}}(k - T_{\text{R2L}})) \\ &- E^3_{\text{L2R}}(k) - E^{\text{PC1}}(k-1), \end{aligned} \tag{3}$$

with the energy E^{PC1} that was already dissipated by $PC1$. The reader is referred to [6] for more details on passivity control. The force scalings $\nu, \mu \in \mathbb{R}$ with $\nu, \mu \in [0,1]$ and $\nu + \mu = 1$ and their consideration in energy observation and control ensures the energy balance in the multilateral system. A potential energy accumulation at PC2 is prevented by a reset logic presented in Section III-D. Note that the maximum stiffness in the VR should equal the stiffness of the $Ctrl$ to provide a reasonable energy reference. This stiffness is low when compared to haptics applications such that the passivity control of the VR does not result in high jittering.

C. Effect analysis

Analogous to the force-feedback of F_E in the TDPA-HD, the force F_V is zero in free motion situations which leads to a zero power input during free motion. Therefore, during free motion, the CC does not introduce energy and the $PC2$ is not active and does not attenuate the velocity reference, thus, avoiding position drift.

In contact situations, a power results at port 6 due to the measured force feedback. In case the contacting surface was modeled in VR (expected contact), the $PC2$ receives a corresponding input power $E^2_{\text{L2R}}(k - T_{\text{L2R}})$ from port 2. Thus, the $PC2$ will not dissipate energy. In case the contact at the robot side happened unexpectedly (contact with an unknown object which is not modeled in VR), the power input at port 2 is zero ($\dot{E}^2_{\text{L2R}}(k - T_{\text{L2R}}) = 0$). Then, $PC2$ attenuates the reference velocity such that the contact force acting on the unknown object is limited.

D. Implementation and Limitations

Consideration of passivity controller induced drift: The control mechanism of $PC2$ (attenuation of the velocity reference) leads to a position drift in the reference pose ${}^{\mathcal{W}}\mathbf{H}_{R'}$, which is the reference frame $\mathcal{R}'$ defined in the world frame $\mathcal{W}$, with respect to the input device pose ${}^{\mathcal{W}}\mathbf{H}_{\mathcal{I}}$. Analogous to the telenavigation setup in [21], this position drift has to be accounted in the pose of the input device ${}^{\mathcal{W}}\mathbf{H}_{\mathcal{I}^*}$ in the VR. The drift $\Delta\mathbf{H}_{\text{drift}}$ is calculated from the delayed input device pose ${}^{\mathcal{W}}\mathbf{H}^{\text{del}}_{\mathcal{I}}$ (port 5) and the robot reference pose ${}^{\mathcal{W}}\mathbf{H}_{\mathcal{R}'}$ (port 6) after passivity control: $\Delta\mathbf{H}_{\text{drift}}(k) = {}^{\mathcal{I}}\mathbf{H}^{\text{del}}_{\mathcal{W}}(k)\,{}^{\mathcal{W}}\mathbf{H}_{\mathcal{R}'}(k)$. Therefore, the input device pose ${}^{\mathcal{W}}\mathbf{H}_{\mathcal{I}^*}$ in the VR becomes

$${}^{\mathcal{W}}\mathbf{H}_{\mathcal{I}^*}(k) = {}^{\mathcal{W}}\mathbf{H}_{\mathcal{I}}(k)\,{}^{\mathcal{I}}\mathbf{Rot}_{\mathcal{I}^{\text{del}}}(k)\Delta\mathbf{H}^{\text{del}}_{\text{drift}}(k), \tag{4}$$

with ${}^{\mathcal{I}}\mathbf{Rot}_{\mathcal{I}^{\text{del}}} = \begin{bmatrix} {}^{\mathcal{I}}\mathbf{R}_{\mathcal{I}^{\text{del}}} & 0 \\ 0 & 1 \end{bmatrix}$ calculated on the operator side. Note that the experiments below show that the drift is already cearly reduced for low μ-values of 0.2 and that moving the robot more slowly with increasing delay and at constant velocities helps reducing the drift.

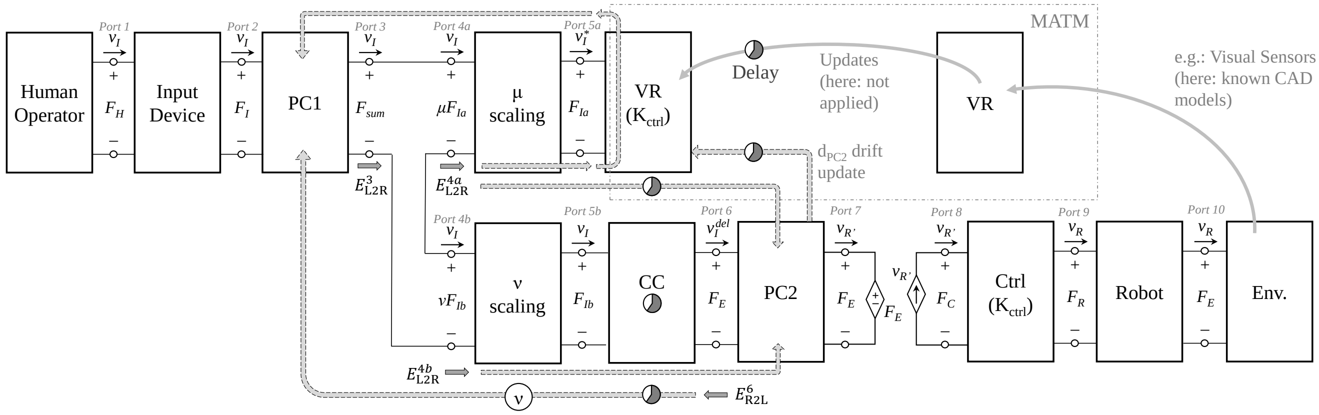

Fig. 9: Network Representation of TDPA-HD with MATM energy reference and combined force feedback: A VR and two scaling subsystems are introduced into the operator-side circuit. The PC2 drift d_{PC2} and potential model updates are exchanged through the communication in addition to the control signals and energies of TDPA-HD.

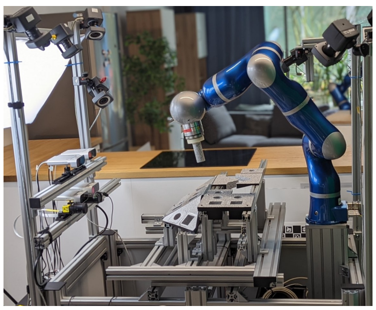

Fig. 10: Light-weight robot (DLR)

Fig. 11: Lambda.7 (Force Dimension)

Combined force feedback (μ and ν): To ensure that the operator is able to interact with non-modeled objects (with $t_{\mathrm{TI}} = T_{\mathrm{L2R}} + T_{\mathrm{R2L}}$) if desired, a combination of measured force feedback F_E and fictitious force feedback F_V should be displayed to the operator such that E^2_{L2R} can be non-zero in case of non-modeled objects. Therefore, we apply the weighted force feedback sum of $\nu F_V(k) + \mu F_E^{\mathrm{del}}(k)$ to the input device. The resulting multilateral control setup is analogous to [21]. If an object is not modeled, the interaction remains passive since E^2_{L2R} is calculated from v_I and $\nu F_V(k) + \mu F_e^{\mathrm{del}}(k)$. In this case, $PC2$ limits the interaction with the non-modeled object with respect to μF_E^{del}.

Avoiding energy accumulation at $PC2$: Since $PC2$ considers E^2_{L2R} as input energy and E^6_{L2R} as output energy at port 6, energy can accumulate in $W^{\mathrm{PC2}}_{\mathrm{obs}}$ since $abs(F_V)$ is potentially higher than $abs(F_E)$. In order to ensure that no energy is accumulated, we reset the energy E_{out} of $PC2$ on the robot side to $E_{\mathrm{out}}(k) = E^2_{\mathrm{L2R}}(k - T_{\mathrm{L2R}}) - E^{\mathrm{PC2}}(k-1)$ when no contact with real and virtual environment is recognized.

Model Updates: In case of active environments, or movable objects, model updates need to be considered. To guarantee stability, these updates should be performed in a passive manner. As a simple solution, updates can be performed during no-contact phases. Alternatively, damping injection methods as in [22] can be applied. In future, we will investigate the combination with the deflection-domain passivity approach (DDPA) of [23]. The DDPA can limit the release of energy from the local VR to the operator according to the potential energy of the remote coupling, for example, through adaptation of the local VR stiffness.

Sensor noise: Due to the noise of the force-torque sensor, a deadband needs to be implemented in which no contact is accounted. Depending on the sensor quality, a low-pass filter may need to be used to reduce the required deadband which was not necessary in the presented experiments. Such filters should be used with caution during telemanipulation, since they cause an additional phase shift. The larger the deadband, the higher is the force that a robot will apply during unexpected contacts.

Energy leaks in haptic rendering: The rendering of virtual forces can introduce energy into the system leading to unstable oscillations. In particular, discrete-time sampling and quantization effects are known to be potential sources of instability in haptics [24], [25]. Two main strategies can be followed to accommodate this problem: a parameter design according to stability analysis for haptic rendering [26] or a passivation of the VR port by introducing a separate TDPA [27]. The position of $PC1$ of the present work results in a setup similar to [27]. Still, note that since the modeled VR stiffness should equal the comparably low $Ctrl$ stiffness, no critical energy injection due to quantization effects is expected.

IV. Experimental Evaluation

The following experiments were performed with the DLR light-weight robot and the Force Dimension lambda.7 presented in Fig. 10 and Fig. 11 respectively. The haptic rendering was realized using the volumetric algorithm VPS [20]. The VR was used for haptic rendering, but not for visualization purposes. The robot equipped with a 3D printed tool interacts with a 3D printed environment. The respective CAD models are utilized for haptic rendering with a god-object heuristic, with which collisions behave like linear springs in the direction of the collision. The control algorithm was implemented in Matlab/Simulink and running at 1kHz sampling rate.

Throughout the evaluation, the scaling was varied: $\mu \in [0, 0.2, 0.5, 0.8]$. The FT sensor deadbands of the TDPA-HD were chosen as $F_{\mathrm{db}} = 0.2N$ and $T_{\mathrm{db}} = 0.05Nm$ for subjectively rated best performance. The force F_I after $PC1$ was filtered with a lowpass-filter at a cutoff frequency of 10Hz This range was chosen according to the maximum frequency

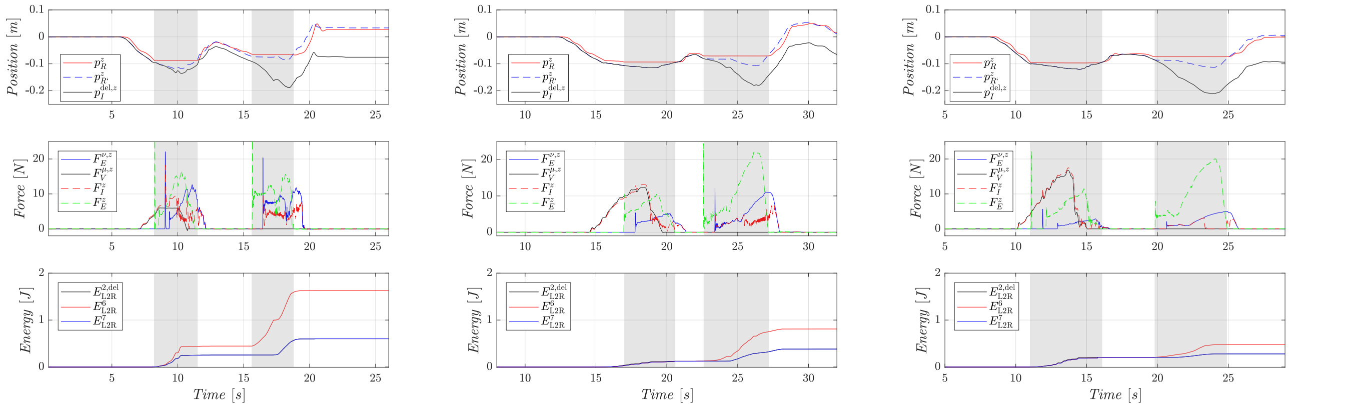

(a) $\mu = 0.2$. **(b)** $\mu = 0.5$. **(c)** $\mu = 0.8$.

Fig. 12: TDPA-HD with MATM: two contacts in VR and real environment in z-direction at 1.6s RTD and various μ-values: the difference between pose of the haptic device p_I^z and the robot reference pose $p_R'^z$ indicates the drift which reduces with increase of μ during the first known contact. $F_E^{\nu,z} = \nu F_{Ib}^z$ is the delayed environment force scaled by ν. $F_V^{\mu,z} = \mu F_{Ia}^z$ is the scaled haptic rendering force.

of user inputs. The haptic rendering stiffness was matched with the stiffness of the coupling controller such that F_{Ia} matches F_R (in case of zero delay and perfect modeling).

A. Abstract 1-DoF evaluation

The results of the initial abstract analysis at 1.6s roundtrip-delay (RTD) are presented in Fig. 12. For the sake of simplicity, only the z-direction is presented at first. Note that, initially, the positions are set to zero for ease of analysis. The first interaction with the environment is a contact with an object modeled in VR, whereas the object of the second contact was not modeled. To reach the second contact, the robot was moved in x-direction. The position of the environmental contacts are analogous to the TDPA-HD experiment of Fig. 5.

The effect of the proposed approach can be most obviously observed from the position drift during the first (modeled) wall contact (difference between p_I and $p_{R'}$) that decreases with increasing μ. Note that the drift during the second (non-modeled) wall contact equals as expected for all experiments of Fig. 5 and Fig. 12. This drift is desired since it reduces the severity of unexpected collisions. As can be analyzed from the energy plots, no energy is accumulated on the robot side ($E^6_{\text{L2R}} = E^2_{\text{L2R}}$). Slight energy resets can be observed after the first wall contacts. Regarding the force plots, the profile of the force F_E during the first contact and the respective amplitude is relevant. Especially, the profile of Fig. 5, but also of Fig. 12a is affected by the drift such that the interaction with the environment is built up more slowly. At the same time, at these low μ-values ($\mu = 0$,$\mu = 0.2$), the force amplitude of F_E is higher than the force displayed at the input device F_I. The match between F_E and F_I improves already with $\mu = 0.2$ in Fig. 12a during the pressing phase of the wall contact. This is also due to the fact that $PC1$ attenuates the force $F_E^{\nu,z}$ to F_I^z most heavily at $\mu = 0$ in Fig. 5. Note that in all experiments mainly the delayed force component is attenuated by $PC1$. Regarding the experiments with $\mu = 0.5$ and $\mu = 0.8$, the safety during contacts is further improved since the profile of F_E is closer to F_I and since F_I is perceived on the operator side before F_E can be applied against the environment such that the wall penetration is decreased in comparison with $\mu = 0$ and $\mu = 0.2$. Overall, with increasing μ, the $PC1$ artifacts are less perceivable.

B. Multi-DoF interaction

The experiment of Fig. 13 to Fig. 14 presents a more complex 6-DoF interaction serving the evaluation of the proposed control method in the three translational dimensions at 1.6s RTD and $\mu = 0.5$. All contacts of this experiment were modeled in VR. As can be analyzed from the position plots of Fig. 13, the operator first commands a contact in z-direction ($t = [9.5s, 12.8s]$). Then, the operator enters a hole in z-direction where a wall contact is first established in y-direction at $t = [17.9s, 26.3s]$ and later in x-direction at $t = [22.1s, 26.3s]$. From the small difference between p_I and $p_{R'}$, it can be concluded that the drift is relatively low regarding the high RTD of 1.6s. As visible from Fig. 14, the force displayed at the input device F_I represents the interaction forces well. A solution to the high F_E during the first contact is discussed later.

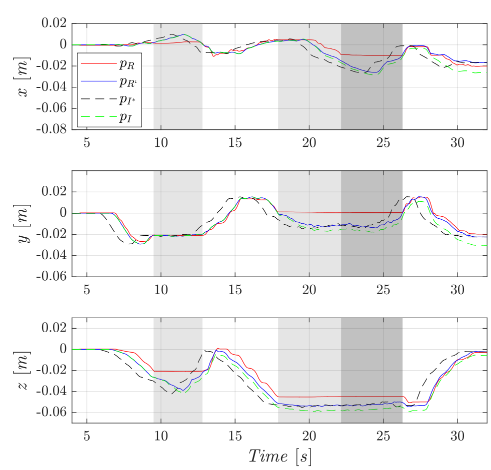

Fig. 13: Multi-DoF experiment at 1.6s RTD and $\mu = 0.5$: Translations.

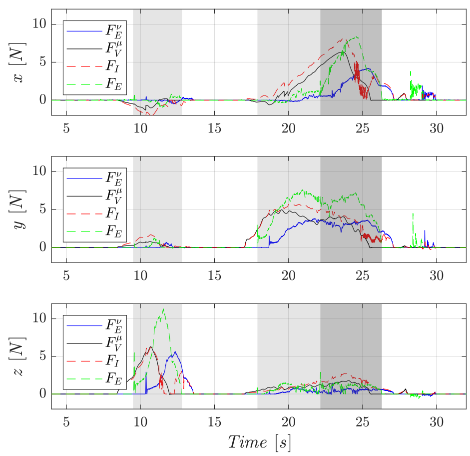

Fig. 14: Multi-DoF experiment at 1.6s RTD and $\mu = 0.5$: Forces.

The rotations are skipped here since the torques generated by the haptic rendering algorithm provide only limited information on the experimental task. Still, the drift compensation and passivity controller are functional in 6-DoF such that the proposed approach is directly applicable to more advanced torque rendering algorithms. Note that the influence of rotational motion or torques on the translations has already been clearly described in the experimental design.

C. Interaction with variable environments

An important manipulation aspect is the interaction with variable environments. In order to validate the control approach with variable environments, in the following, a simulated local spring (stiffness K_l at wall position x_l) and remote spring (K_r at x_r) are applied. To test the effects of modelling inaccuracies, different spring offsets ($x_l \neq x_r$) and different stiffness values ($K_l \neq K_r$) are considered in the experiments of Fig. 15.

Comparing the plot for pure TDPA-HD ($\mu = 0$) in Fig. 15a with the proposed approach in Fig. 15b at $\mu = 0.5$, the drift is much higher in case of $\mu = 0$ (visualized by the difference $d_{\text{PC2}} = p_I^{\text{del}} - p_{R'}$). Thus, also the force F_E builds up faster at $\mu = 0.5$ in Fig. 15b.

In case of Fig. 15c and Fig. 15f, the modeled wall is 2cm more distant from the operator than the real wall. It can be observed that due to the delay, energy still arrives early enough to build up the remote interaction faster than for $\mu = 0$. In the experiment of Fig. 15f with reduced stiffness K_l, the force F_E is much higher than the perceived force F_I. This result indicates that the operator moves less carefully since a low stiffness was perceived locally. For the sake of safety, the force F_R commanded to the robot should be limited to $\mu F_{Ia}^{\text{del}} + \nu F_E$ such that the operator is aware of the applied force. Also regarding the other performed experiments, this limitation would not lead to a critical reduction of performance and clearly increase safety of interactions. Comparing the experiments with modeled walls that are closer than the real walls (compare Fig. 15d and Fig. 15e), F_E corresponds better with F_I despite increased stiffness in Fig. 15e. This is probably due to the fact that the remote spring is deflected less because of the earlier and/or increased local resistance against motion.

D. Discussion

Overall, the results confirm the functionality of the approach. The drift is clearly reduced and the remote interaction is built up faster already at low μ (see Fig. 12a). To increase safety in case of modeling errors, a limitation of F_R to $\mu F_{Ia}^{\text{del}} + \nu F_E$ might be required. This limitation of F_R as well as the parametrization of ν and μ should be chosen according to the confidence in the environment modeling and the haptic rendering algorithm. The safety of TDPA-HD in case of unexpected collisions was maintained under the proposed MATM-based approach.

V. Conclusion and Future work

This work presented a model-augmentation-based method reducing the time-to-interact of a teleoperated remote robot. The method was applied with the TDPA-HD enabling teleoperation at extreme delays. The experiments showed that the new concept can reduce the time until the robot applies forces on an object after first contact (time-to-interact) by one round-trip delay (i.e. by more than 50%) while preserving the safety in the interaction. This benefit was also confirmed in case of modeling errors and flexible environments.

In future work, torque rendering should be investigated in detail allowing for the evaluation in rotational DoFs. Furthermore, the integration of point-cloud-based VRs will render the approach more suitable to unknown environments. Another research direction may focus on real-time impedance calculation of the environment, adaptive μ-scaling and on the integration of a physics engine to perform multi-body interactions.

References

[1] N. Y. Lii, C. Riecke, D. Leidner, S. Schätzle, P. Birkenkampf, B. Weber, T. Krueger, M. Stelzer, A. Wedler, and G. Grunwald. The robot as an avatar or co-worker? An investigation of the different teleoperation modalities through the Kontur-2 and METERON SUPVIS Justin space telerobotic missions. In *The Interanational Astronautical Congress (IAC)*. IAF, 2018.

[2] R Ambrose, IAD Nesnas, F Chandler, BD Allen, T Fong, L Matthies, and R Mueller. NASA technology roadmaps: Ta 4: Robotics and autonomous systems. In *National Aeronautics and Space Administration (NASA), NASA Headquarters*, 2015.

[3] Jack O Burns, Benjamin Mellinkoff, Matthew Spydell, Terrence Fong, David A Kring, William D Pratt, Timothy Cichan, and Christine M Edwards. Science on the lunar surface facilitated by low latency telerobotics from a lunar orbital platform-gateway. *Acta Astronautica*, 154:195–203, 2019.

[4] Kjetil Wormnes, William Carey, Thomas Krueger, Leonardo Cencetti, Emiel den Exter, Stephen Ennis, Edmundo Ferreira, Antonio Fortunato, Levin Gerdes, Lukas Hann, et al. Analog-1 iss-the first part of an analogue mission to guide esa's robotic moon exploration efforts. In *Global Space Exploration Conference (GLEX 2021)*, 2021.

[5] Michael Panzirsch, Harsimran Singh, Thomas Krüger, Christian Ott, and Alin Albu-Schäffer. Safe Interactions and Kinesthetic Feedback in High Performance Earth-To-Moon Teleoperation. In *IEEE Aerospace Conference*, 2020.

[6] Michael Panzirsch, Aaron Pereira, Harsimran Singh, Bernhard Weber, Edmundo Ferreira, Andrei Gherghescu, Lukas Hann, Emiel den Exter, Frank van der Hulst, Levin Gerdes, et al. Exploring planet geology through force-feedback telemanipulation from orbit. *Science Robotics*, 7(65):eabl6307, 2022.

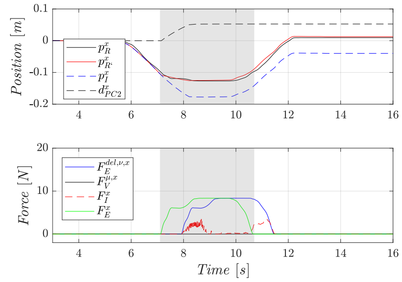

(a) TDPA-HD: $\mu = 0$, $K_r = 300\ N/m$, $x_r = x_l$.

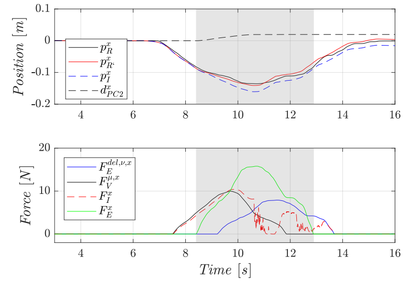

(b) TDPA-HD with MATM: $\mu = 0.5$, $K_r = K_l = 300N/m$, $x_r = x_l$.

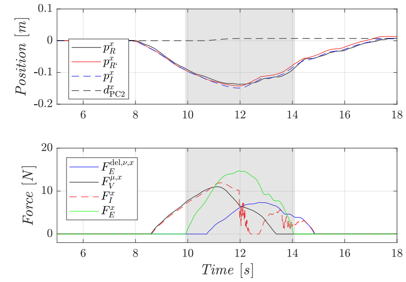

(c) TDPA-HD with MATM: $\mu = 0.5$, $K_r = K_l = 300N/m$, $x_r = x_l$+0.02m.

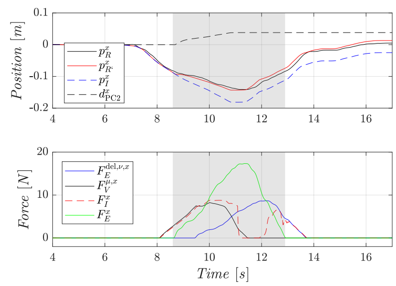

(d) TDPA-HD with MATM: $\mu = 0.5$, $K_r = K_l = 300N/m$, $x_r = x_l$-0.02m.

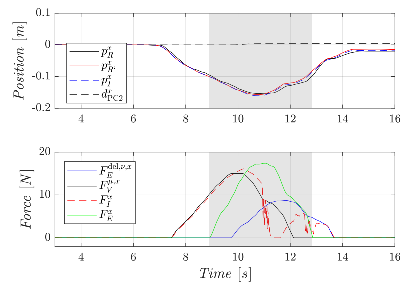

(e) TDPA-HD with MATM: $\mu = 0.5$, $K_l = K_r$+100$N/m = 400N/m$, $x_r = x_l$-0.02m.

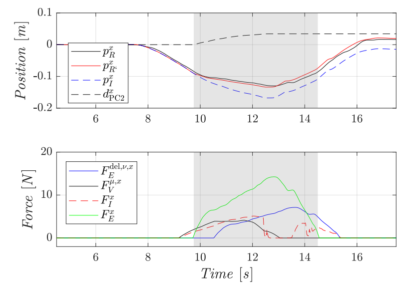

(f) TDPA-HD with MATM: $\mu = 0.5$, $K_l = K_r$-100$N/m = 200N/m$, $x_r = x_l$+0.02m.

Fig. 15: Evaluation with simulated variable environment.

[7] Ribin Balachandran, Jordi Artigas, Usman Mehmood, and Jee-Hwan Ryu. Performance comparison of wave variable transformation and time domain passivity approaches for time-delayed teleoperation: Preliminary results. In *Proceedings of 2016 IEEE/RSJ International Conference on Intelligent Robots and Systems*, pages 410–417. IEEE, 2016.

[8] Jee-Hwan Ryu, Jordi Artigas, and Carsten Preusche. A passive bilateral control scheme for a teleoperator with time-varying communication delay. *Mechatronics*, 20(7):812–823, 2010.

[9] Takashi Imaida, Yasuyoshi Yokokohji, Toshitsugu Doi, Mitsushige Oda, and Tsuneo Yoshikawa. Ground-space bilateral teleoperation of ets-vii robot arm by direct bilateral coupling under 7-s time delay condition. *IEEE Transactions on Robotics and Automation*, 20(3):499–511, 2004.

[10] Michael Panzirsch and Harsimran Singh. Position synchronization through the energy-reflection based time domain passivity approach in position-position architectures. *IEEE Robotics and Automation Letters*, 6(4):7997–8004, 2021.

[11] Thomas Hulin, Michael Panzirsch, Harsimran Singh, Ribin Balachandran, Andre Coelho, Aaron Pereira, Bernhard M Weber, Nicolai Bechtel, Cornelia Riecke, Bernhard Brunner, et al. Model-augmented haptic telemanipulation: Concept, retrospective overview and current use-cases. *Frontiers in Robotics and AI*, 8:76, 2021.

[12] Ryo Suzuki, Adnan Karim, Tian Xia, Hooman Hedayati, and Nicolai Marquardt. Augmented reality and robotics: A survey and taxonomy for ar-enhanced human-robot interaction and robotic interfaces. In *Proceedings of the 2022 CHI Conference on Human Factors in Computing Systems*, pages 1–33, 2022.

[13] David Valenzuela-Urrutia, Rodrigo Muñoz-Riffo, and Javier Ruiz-del Solar. Virtual reality-based time-delayed haptic teleoperation using point cloud data. *Journal of Intelligent & Robotic Systems*, 96:387–400, 2019.

[14] Dejing Ni, Andrew YC Nee, Soh-Khim Ong, Huijun Li, Chengcheng Zhu, and Aiguo Song. Point cloud augmented virtual reality environment with haptic constraints for teleoperation. *Transactions of the Institute of Measurement and Control*, 40(15):4091–4104, 2018.

[15] Xiao Xu, Burak Cizmeci, Anas Al-Nuaimi, and Eckehard Steinbach. Point cloud-based model-mediated teleoperation with dynamic and perception-based model updating. *IEEE Transactions on Instrumentation and Measurement*, 63(11):2558–2569, 2014.

[16] Yongqing Fu, Weiyang Lin, Xinghu Yu, Juan J Rodríguez-Andina, and Huijun Gao. Robot-assisted teleoperation ultrasound system based on fusion of augmented reality and predictive force. *IEEE Transactions on Industrial Electronics*, 2022.

[17] Chao Liu, Jing Guo, and Philippe Poignet. Nonlinear model-mediated teleoperation for surgical applications under time variant communication delay. *IFAC-PapersOnLine*, 51(22):493–499, 2018.

[18] Thiago Weber Martins, Aaron Pereira, Thomas Hulin, Oliver Ruf, Stefan Kugler, Alessandro Giordano, Ribin Balachandrand, Fabian Benedikt, John Lewis, Reiner Anderl, et al. Space factory 4.0-new processes for the robotic assembly of modular satellites on an in-orbit platform based on 'industrie 4.0' approach. In *Proceedings of the International Astronautical Congress, IAC*, 2018.

[19] Kenneth Salisbury, Francois Conti, and Federico Barbagli. Haptic rendering: introductory concepts. *IEEE computer graphics and applications*, 24(2):24–32, 2004.

[20] Mikel Sagardia and Thomas Hulin. Multimodal evaluation of the differences between real and virtual assemblies. *IEEE transactions on haptics*, 11(1):107–118, 2017.

[21] Michael Panzirsch, Harsimran Singh, Martin Stelzer, Martin J Schuster, Christian Ott, and Manuel Ferre. Extended predictive model-mediated teleoperation of mobile robots through multilateral control. In *2018 IEEE Intelligent Vehicles Symposium (IV)*, pages 1723–1730. IEEE, 2018.

[22] Xiao Xu, Clemens Schuwerk, and Eckehard Steinbach. Passivity-based model updating for model-mediated teleoperation. In *2015 IEEE International Conference on Multimedia & Expo Workshops (ICMEW)*, pages 1–6. IEEE, 2015.

[23] Michael Panzirsch, Marek Sierotowicz, Revanth Prakash, Harsimran Singh, and Christian Ott. Deflection-domain passivity control of variable stiffnesses based on potential energy reference. *IEEE Robotics and Automation Letters*, accepted, 2022.

[24] Jake J Abbott and Allison M Okamura. Effects of position quantization and sampling rate on virtual-wall passivity. *IEEE Transactions on Robotics*, 21(5):952–964, 2005.

[25] Nicola Diolaiti, Günter Niemeyer, Federico Barbagli, and J Kenneth Salisbury. Stability of haptic rendering: Discretization, quantization, time delay, and coulomb effects. *IEEE Transactions on Robotics*, 22(2):256–268, 2006.

[26] Thomas Hulin, Alin Albu-Schäffer, and Gerd Hirzinger. Passivity and stability boundaries for haptic systems with time delay. *IEEE Transactions on Control Systems Technology*, 22(4):1297–1309, 2013.

[27] Katharina Hertkorn, Thomas Hulin, Philipp Kremer, Carsten Preusche, and Gerd Hirzinger. Time domain passivity control for multi-degree of freedom haptic devices with time delay. In *2010 IEEE International Conference on Robotics and Automation*, pages 1313–1319. IEEE, 2010.